The Morphology of the Tasmantid Seamounts: Interactions between Tectonic Inheritance and Magmatic Evolution

B487 - 10857

Fred Richards[1, 2*], Lara Kalnins[3], Tony Watts[1], Benjamin Cohen[4] & Rob Beaman[5]

[1]Department of Earth Sciences, University of Oxford, Oxford, UK [2]Bullard Laboratories, Department of Earth Sciences, University of Cambridge, Cambridge, UK [3]Department of Earth Sciences, University of Durham, UK
[4]Scottish Universities Environment Research Centre, East Kilbride, UK [5]College of Science, Technology and Engineering, James Cook University, Cairns, Australia

*fdr22@cam.ac.uk

1 Introduction

The Tasmantid seamounts extend for over 2000 km off the east coast of Australia and constitute one of three contemporaneous, sub-parallel Cenozoic hotspot tracks that traverse the region, locally separated by less than 500 km (Cohen *et al.*, 2013). Together, these chains constitute the East Australian Plume System and, where dated, young from north to south, spanning ~34-6 Ma (McDougall & Duncan, 1988). At multiple locations, the Tasmantid chain intersects the extinct slow-spreading Tasman Sea ridge system, which was active from 84 Ma to 53 Ma (Müller et al., 2008). Despite the spreading cessation pre-dating seamount emplacement by >20 Ma, palaeo-ridge structure appears to be a major control on seamount morphology.

Analysis of geophysical datasets acquired on the TMD2012 cruise (1), together with publicly available datasets*, has been undertaken in order to answer the following questions:

- What mechanisms account for the morphological diversity of the seamounts?
- What does the relationship between pre-existing tectonic fabric and intraplate magmatism suggest about the structure and long-term strength of the Tasman Sea lithosphere?
- What information about the the magnitude and variability of the Tasmantid melting anomaly can be gleaned from observed volcanic architecture?

*GBR100 bathymetry grid (Beaman, 2010) & global satellite free-air gravity grid (Sandwell & Smith, 2009)

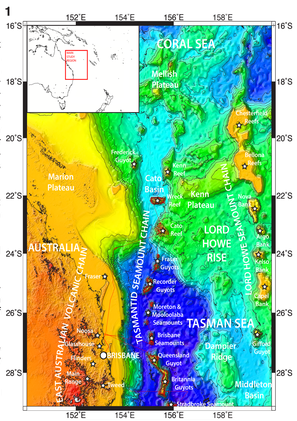

Figure 1. Bathymetry map of the study area. Red line = shiptrack of RV Southern Surveyor cruise TMD2012. White stars = positions of major seamounts/volcanoes inferred to relate to the East Australian Plume System.

2 Slope Analysis

The diversity in volcanic form observed across the chain is clearly reflected in their slope characteristics with tectonic setting apparently the controlling factor – conical seamounts with elevated slope gradients but lower intersector variance occur off-axis and at outside corners (**2a)**); rugged seamounts with low slope gradient but high intersector variability occur at inside corners (**2d)**). Terraced and shield seamounts have distinctively variable and low gradient upper slopes suggesting elevated rates of mass wasting related to sub-aerial exposure (**2b)** & **2c)ii)**).

Overall the seamounts display high slope gradients, low intersector slope variance and elevated backscatter readings, indicating that large mass-wasting events are generally rare (**3**). This is consistent with minimal shallow deformation and may reflect modest eruption rates with a high intrusive-to-extrusive magmatic budget (Ramalho *et al.*, 2013).

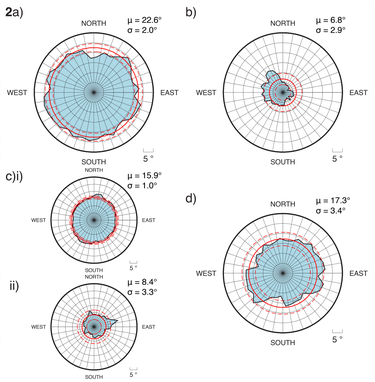

Figure 2. Average slope gradient by sector. **a)** South Moreton, a conical seamount. **b)** Cato, a shield seamount. **c)** Britannia, a terraced seamount. **i)** slopes from deepest wave-cut terrace to basal contour, **ii)** slopes from summits to lowest terrace. **d)** Stradbroke, a rugged seamount.

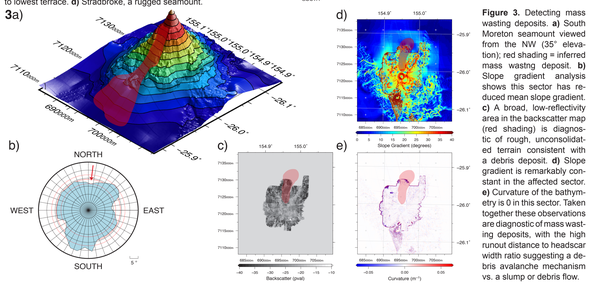

Figure 3. Detecting mass wasting deposits. **a)** South Moreton seamount viewed from the NW (35° elevation); red shading = inferred mass wasting deposit. **b)** Slope gradient analysis shows this sector has reduced mean slope gradient. **c)** A broad, low-reflectivity area in the backscatter map (red shading) is diagnostic of rough, unconsolidated terrain consistent with a debris deposit. **d)** Slope gradient is remarkably constant in the affected sector. **e)** Curvature of the bathymetry is 0 in this sector. Taken together these observations are diagnostic of mass wasting deposits, with the high runout distance to headscar width ratio suggesting a debris avalanche mechanism vs. a slump or debris flow.

3 Deep Structure

To investigate subsurface mass distributions, predicted gravity effects of the water-sediment and sediment-edifice interfaces were calculated using a 5th order Parker expansion FFT method (**4a)**, **b)**, **e)**) and subtracted from free-air anomalies (**4c)**, **e)**) to generate Bouguer anomalies (**4e)**, **f)**). Basement densities were chosen to minimise coherence between topography and Bouguer anomalies (**4d)**, **e)**). The 20-50 mGal Bouguer highs over the centres of many edifices (**4f)**) suggest extensive intra-basement intrusion of primary magmas – they persist for basement densities >3000 kg/m^3 – and sluggish rates of extraction. This is consistent with minimal surface disturbance and observed scarcity of mass-wasting deposits (Contreras-Reyes *et al.*, 2010).

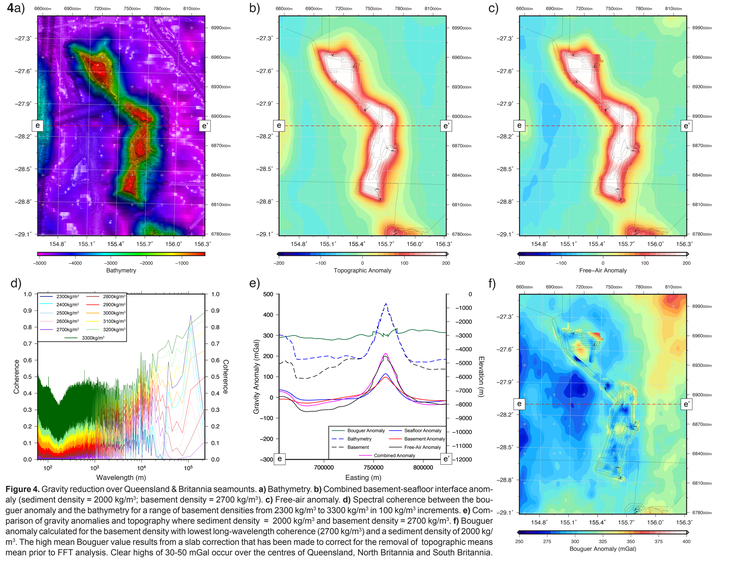

Figure 4. Gravity reduction over Queensland & Britannia seamounts. **a)** Bathymetry. **b)** Combined basement-seafloor interface anomaly (sediment density = 2000 kg/m^3; basement density = 2700 kg/m^3). **c)** Free-air anomaly. **d)** Spectral coherence between the bouguer anomaly and the bathymetry for a range of basement densities from 2300 kg/m^3 to 3300 kg/m^3 in 100 kg/m^3 increments. **e)** Comparison of gravity anomalies and topography where sediment density = 2000 kg/m^3 and basement density = 2700 kg/m^3. **f)** Bouguer anomaly calculated for the basement density with lowest long-wavelength coherence (2700 kg/m^3) and a sediment density of 2000 kg/m^3. The high mean Bouguer value results from a slab correction that has been made to correct for the removal of topographic means mean prior to FFT analysis. Clear highs of 30-50 mGal occur over the centres of Queensland, North Britannia and South Britannia.

4 Modelling Lithospheric Strength

Forward modelling of seamount gravity anomalies was undertaken to assess the lithospheric strength of the Tasman Sea. Modelling efforts were complicated by thick sediment cover requiring joint calculation of sediment and seamount loading combined with a lack of seismic constraint on basement and Moho interfaces. However, preliminary results point to the absence of a relationship between T_e and age of oceanic crust at time of loading (**5a)**).

Rugged seamounts emplaced on inside corners and fracture zones generally exhibit low T_e suggesting that extensive faulting weakens the lithosphere in these settings, thereby obliterating any underlying plate strengthening trend associated with plate cooling (c.f. Watts & Zhong, 2000). Tectonic setting, not plate age, is therefore the determining factor for Tasman Sea lithospheric strength.

Bouguer anomaly maps exhibit residual highs over edifice centres (**4f)**). Gravity modelling suggests that these anomaly amplitudes can only be matched if dense cores (2900 kg/m^3) and substantial intrabasement intrusions (3000 kg/m^3) are invoked (**5b)**).

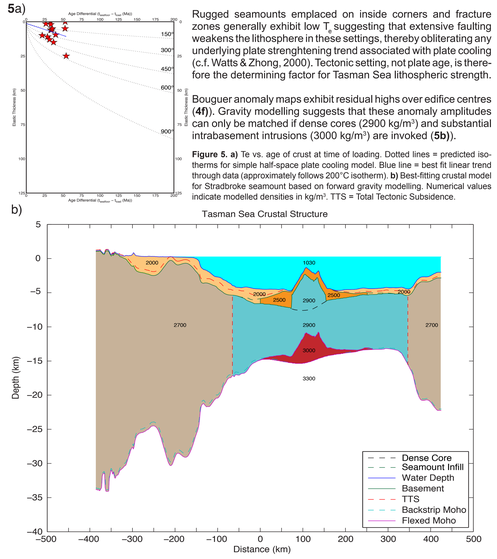

Figure 5. a) Te vs. age of crust at time of loading. Dotted lines = predicted isotherms for simple half-space plate cooling model. Blue line = best fit linear trend through data (approximately follows 200°C isotherm). **b)** Best-fitting crustal model for Stradbroke seamount based on forward gravity modelling. Numerical values indicate modelled densities in kg/m^3. TTS = Total Tectonic Subsidence.

5 Volcanic Architecture

Tasmantid morphologies fall into four distinct categories: i) rugged seamounts constructed via repeated fissure eruptions along crosscutting volcanic rift zones (VRZs) (**6a)**); ii) shield seamounts with shallow slopes and dispersed cinder cones (**6b)**); iii) elongated, terraced seamounts with subaerially eroded peaks (**6c)** & **d)**) and iv) conical seamounts characterised by summit calderas and smooth flanks (**6e)** & **f)**). The chain exhibits low rates of mass wasting, highly variable VRZ orientation and fluctuating edifice volume, with morphology varying dramatically between seamounts separated by as little as 10 km. Plotting multibeam bathymetry against tectonic context shows a clear link between overall morphology and seamount position relative to ridge structure.

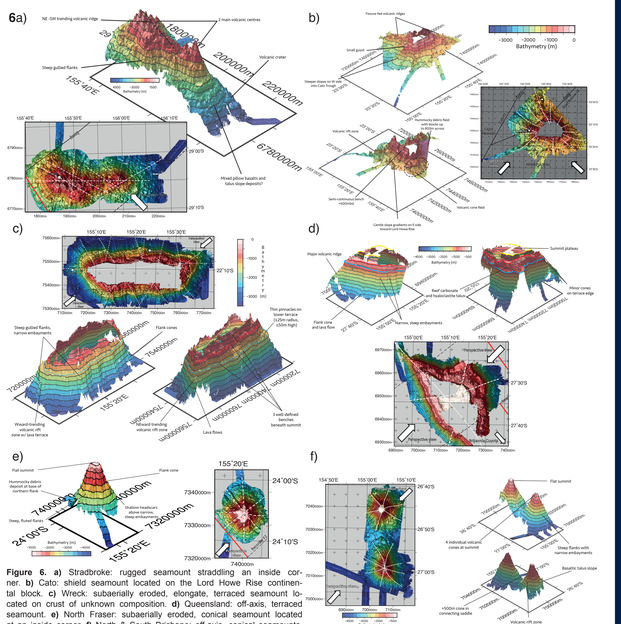

Figure 6. a) Stradbroke: rugged seamount straddling an inside corner **b)** Cato: shield seamount located on the Lord Howe Rise continental block. **c)** Wreck: subaerially eroded, elongate, terraced seamount located on crust of unknown composition. **d)** Queensland: off-axis, terraced seamount. **e)** North Fraser: subaerially eroded, conical seamount located at an inside corner. **f)** North & South Brisbane: off-axis, conical seamounts.

6 Structural Orientations

VRZs, faults and long axes of faults were delineated using bathymetry data with consistent orientations emerging amongst seamounts emplaced in specific tectonic settings (**7** & **8**). Seamounts located at inside corners have major trends oblique to spreading trends implying that strong mechanical coupling characterised the transform faults, consistent with slow spreading and reduced magma supply (**9**). Observed alignments suggest deep faulting of the oceanic lithosphere allowing channelisation of magma along pre-existing structural trends, despite the intraplate volcanism postdating active extension by >20Ma. The dominance of the tectonic signal, from surface expressions (**Box 2**, **5** & **6**) through to lithospheric structure (**Box 3** & **4**), points to low melt production, implying that the Tasmantid "plume" may have constituted a relatively weak mantle anomaly.

Figure 7. Orientations of linear features vs. tectonic context at individual seamounts. **a)** Stradbroke, rugged edifice; **i)** major trends oblique-to-spreading and **ii)** inside-corner setting. **b)** South and North Recorder terraced edifices; **i)** South Recorder has volcanic trends parallel to Recorder Fracture Zone and **iii)** fracture zone setting; **ii)** North Recorder has ridge-parallel lineaments and **iii)** off-axis setting. **c)** North Fraser, conical edifice; **i)** principal trends ridge-parallel and subparallel to fracture zones and **ii)** outside corner setting. Red = major VRZs and elongation axes, blue = minor VRZs and black = faults. IC = inside corner; OC = outside corner. **Figure 8.** Summary of linear feature orientation vs. tectonic setting for whole chain. **a)** Axial ridges (red) and fracture zones (black). **b)** Inside corner seamounts. **c)** Fracture zone seamounts. **d)** Continental seamounts. **e)** Outside corner seamounts. **f)** Off-axis seamounts. Colour scheme same as **8**.

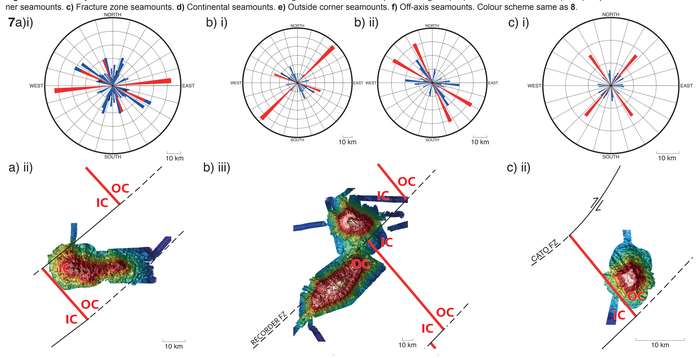

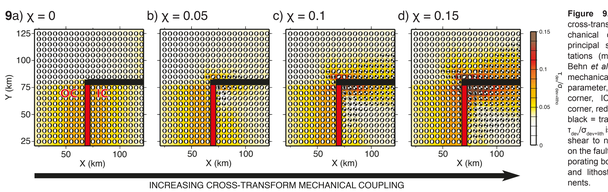

Figure 9. Effect of cross-transform mechanical coupling on principal stress orientations (modified after Behn *et al.*, 2002). χ = mechanical coupling parameter, OC = inside corner, IC = outside corner, red = ridge axis, black = transform fault. $\sigma_{3max}/\sigma_{1max}$ is the ratio of shear to normal stress on the fault plane incorporating both deviatoric and lithostatic components.

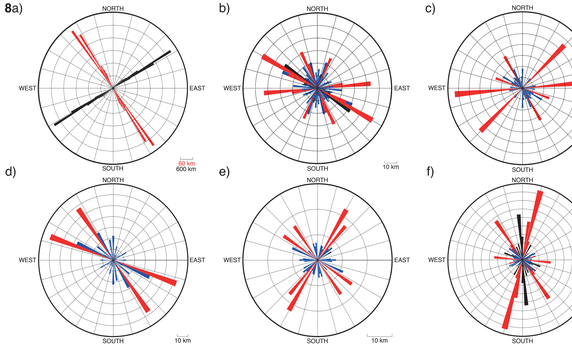

7 Conclusions

1) Morphology varies dramatically between seamounts, even those separated by <10km distance.

2) The modest rates of mass wasting revealed by slope analysis combined with the prevalence of dense cores indicated by gravity signatures and lithospheric modelling suggest that subsurface intrusion, rather than sub-aqueous eruption, was the dominant magmatic growth mechanism.

3) Low overall T_e and the >20Ma time separation between seamount emplacement and spreading cessation suggest deep intra-lithospheric faulting must have accompanied spreading in order to allow Tasmantid magmas to exploit and align with pre-existing structural weaknesses.

4) The slow rate of magma supply, as indicated by the dominance of tectonic controls, high intrusive:extrusive ratios and scarcity of large mass-wasting deposits, points to a relatively weak Tasmantid melting anomaly.

5) Tectonic inheritance is the dominant control on the magmatic evolution of the Tasmantid chain as demonstrated by: a) dependence of morphology on tectonic setting; b) absence of a T_e–age relationship and c) strong alignment of volcanic features at all depths with principal stress directions predicted for the Tasman Sea ridge system.

6) The strong dependence of intraplate magmatic fabric on ridge setting, long after cessation of active spreading, demonstrates the importance of understanding tectonic inheritance in predicting the behaviour of magmatic systems globally.

8 References

Beaman, R. J. (2010). MTSRF Project 2.5i.1a Final Report, Reef and Rainforest Research Centre, Cairns, Australia, pp. 13 & Appendix 1.
Behn M. D., Lin J. & Zuber M. T. (2002), Evidence for weak oceanic transform faults, *Geophys. Res. Lett.*, **29**(24), 2207.
Cohen B. E., Knesel K.M., Vasconcelos P. M. & Schellart W. P. (2013). Tracking the Australian plate motion through the Cenozoic: constraints from $^{40}Ar/^{39}Ar$ geochronology. *Tectonics*, **32**, pp.1371–1383.
Contreras-Reyes E., Grevemeyer I., Watts A. B., Planert L., Flueh E. R. & Peirce C. (2010). Crustal intrusion beneath the Louisville hotspot track, *Earth Plan. Sci. Lett.*, **289**(3-4), pp. 323-333.
McDougall I. & Duncan R. A. (1988), Age progressive volcanism in the Tasmantid Seamounts, *Earth Plan. Sci. Lett.*, 89, pp. 207-220.
Müller R. D., Sdrolias M., Gaina C. & Roest W. R. (2008), Age, spreading rates, and spreading asymmetry of the world's ocean crust, *Geochem. Geophys. Geosyst.*, **9**, Q04006.
Ramalho, R. S., Quartau, R., Trenhaile, A. S., Mitchell, N. C., Woodroffe, C. D., & Ávila, S. P. (2013). Coastal evolution on volcanic oceanic islands: A complex interplay between volcanism, erosion, sedimentation, sea-level change and biogenic production. *Earth-Sci. Reviews*, **127**, pp.140–170.
Sandwell, D. T., & W. H. F. Smith (2009), Global marine gravity from retracked Geosat and ERS-1 altimetry: Ridge segmentation versus spreading rate, *J. Geophys. Res.*, **114**, B01411.
Watts, A. B. & Zhong S. (2000), Observations of flexure and the rheology of oceanic lithosphere, *Geophys. J. Int.*, **142**, pp. 855-875.